Design and Analysis of Vector Color Error Diffusion Halftoning Systems

Niranjan Damera-Venkata, *Member, IEEE,* and Brian L. Evans, *Senior Member, IEEE*

***Abstract*—Traditional error diffusion halftoning is a high quality method for producing binary images from digital grayscale images. Error diffusion shapes the quantization noise power into the high frequency regions where the human eye is the least sensitive. Error diffusion may be extended to color images by using error filters with matrix-valued coefficients to take into account the correlation among color planes. For vector color error diffusion, we propose three contributions. First, we analyze vector color error diffusion based on a new matrix gain model for the quantizer, which linearizes vector error diffusion. The model predicts key characteristics of color error diffusion, esp. image sharpening and noise shaping. The proposed model includes linear gain models for the quantizer by Ardalan and Paulos and by Kite *et al.*as special cases. Second, based on our model, we optimize the noise shaping behavior of color error diffusion by designing error filters that are optimum with respect to any given linear spatially-invariant model of the human visual system. Our approach allows the error filter to have matrix-valued coefficients and diffuse quantization error across color channels in an opponent color representation. Thus, the noise is shaped into frequency regions of reduced human color sensitivity. To obtain the optimal filter, we derive a matrix version of the Yule–Walker equations which we solve by using a gradient descent algorithm. Finally, we show that the vector error filter has a parallel implementation as a polyphase filterbank.**

***Index Terms*—Color quantization, halftoning, image display, parallel halftoning.**

I. Introduction

TRADITIONAL grayscale error diffusion halftoning quantizes an eight bit/pixel grayscale image to a one bit/pixel image for reproduction on binary devices. The reproduction is high quality because error diffusion shapes the quantization noise into the high frequencies (a.k.a. "blue noise") where the human visual system is least sensitive [1]. In addition to adding noise, grayscale error diffusion also sharpens the image [2]–[4]. The amount of sharpening depends on the error filter. The twelve-tap Jarvis error filter [5] produces significant image sharpening whereas the four-tap Floyd–Steinberg error filter [6] produces only modest sharpening.

Manuscript received December 22, 1999; revised May 6, 2001. This work was supported by a U.S. National Science Foundation CAREER Award under Grant MIP-9702707. The associate editor coordinating the review of this manuscript and approving it for publication was Prof. Robert L. Stevenson.

N. Damera-Venkata was with the Embedded Signal Processing Laboratory, The University of Texas, Austin, TX 78712 USA. He is now with the Halftoning and Image Processing Group, Hewlett-Packard Laboratories, Palo Alto, CA 94304 USA.

B. L. Evans is with the Embedded Signal Processing Laboratory, Department of Electrical and Computer Engineering, The University of Texas, Austin, TX 78712 USA (e-mail: bevans@ece.utexas.edu).

Publisher Item Identifier S 1057-7149(01)07462-0.

Kite *et al.* [3], [7] quantify the sharpening and noise introduced by grayscale error diffusion by linearizing error diffusion. They replace the quantizer with the linear gain model developed by Ardalan and Paulos [8] for sigma–delta modulation. The model accurately predicts the noise shaping and image sharpening in error diffused halftones. Based on the model, they develop an objective measure of the human visual system response to each type of degradation, and a low-complexity method for compensating the image sharpening. Their analysis assumes that the error filter is fixed.

This paper generalizes the linear system model of grayscale error diffusion in [3] to vector color error diffusion by replacing the linear gain model with a new matrix gain model and by using properties of filters with matrix-valued coefficients. The new model includes the earlier linear gain model [3], [7] as a special case. The new model describes vector color diffusion in the frequency domain, and predicts noise shaping and linear frequency distortion produced by halftoning.

Color error diffusion is a high-quality method for color rendering of *continuous-tone* 24-bit digital color images on devices with limited color palettes such as low-cost displays and printers. The rendered images are commonly referred to as *color halftones*. Quantization errors are filtered using an *error filter* and fed back to the input in order to shape the quantization noise into frequency regions where humans are relatively less sensitive.

Kolpatzik and Bouman [9] and Akarun *et al.* [10] use error filters with matrix-valued coefficients to account for correlation among the color planes. The error filter by Kolpatzik and Bouman [9] filters each color error plane independently in an opponent color space [9]. Separate optimum scalar error filters are designed for the luminance and chrominance channels independently based on a separable model of the human visual system. However, no constraints are imposed on the error filter to ensure that all of the red–green–blue (RGB) quantization error is diffused. Akarun *et al.* [10] adapt the matrix-valued error filter coefficients using a least mean squares algorithm. This allows for cross-channel diffusion of color error. However, their method does not incorporate a human vision model.

In this paper, we derive the optimum matrix-valued error filter using a matrix gain model to model the noise shaping behavior of color error diffusion and a generalized linear spatially-invariant model (not necessarily separable) for the human color vision. We also incorporate the constraint that all of the RGB quantization error be diffused. We show that the optimum error filter may be obtained as a solution to a matrix version of the Yule–Walker equations. A gradient descent algorithm is proposed to solve the generalized Yule–Walker equations.

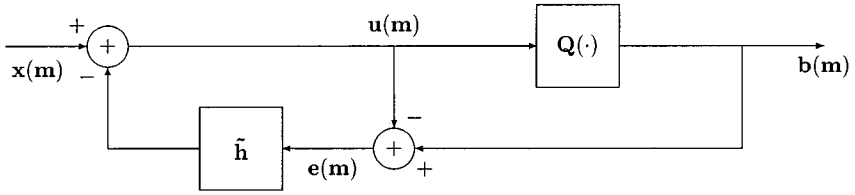

Fig. 1. System block diagrams for block error diffusion halftoning. $\tilde{\mathbf{h}}$ represents a fixed 2-D nonseparable FIR error filter with matrix valued coefficients. The vector $\mathbf{m}$ represents the 2-D index (m_1, m_2).

In the special case when we do not constrain all the error to be diffused, a separable color vision model is used and the linear transformation into the opponent color space is unitary, our solution reduces to the solution derived by Kolpatzik and Bouman [9]. In our formulation based on the matrix gain model, an uncorrelated noise image replaces the highly correlated error image in the objective function in [11], [12]. Because the error filter does not need to minimize correlated signal components, the filter can be solely optimized for noise shaping.

To increase the efficiency of vector color error diffusion, we reorder the computations performed by the error filter (which has matrix-valued coefficients) to derive an equivalent efficient implementation as a polyphase filter bank. Polyphase filter banks are used for efficient parallel implementations of filter banks in digital audio [13]. The implementation of the error filter may be improved up by a factor of three because each of the three color planes being input can be buffered and filtered independently of the other color planes. Such an implementation makes vector color error diffusion attractive for raster image processing.

Section II reviews the mathematical notation used in the paper for scalar, vector, and matrix-valued signals and their transforms. Section III introduces the matrix gain model for vector color error diffusion and validates the model by predicting linear frequency distortion and noise shaping effects of vector color error diffusion. The necessary and sufficient condition to eliminate linear frequency distortion in vector color error diffusion using a prefilter is derived. Section IV designs optimum fixed error filters for vector color error diffusion using the matrix gain model and a model for color appearance. The model for color appearance [14] incorporates human visual sensitivity to color patterns of different spatial frequencies. The color of a pattern is defined according to the model by the excitation of the fundamental cone photoreceptors in the visual system. Thus it is possible to obtain optimal error filters for calibrated imaging devices such as color monitors. Section V derives a parallel implementation for an error filter with matrix-valued coefficients. Section VI concludes the paper by summarizing the contributions.

II. Notation

A. General Notation

In this paper, boldface quantities written with a ˜ represent matrices, whereas boldface quantities written without a ˜ represent vectors. Capitalized quantities are in the frequency domain while lower case quantities are in the spatial domain. Scalar quantities are represented as usual as plain characters. The ith component of a vector $\mathbf{a}$ will be denoted by a_i whereas the (i, j)th element of a matrix $\tilde{\mathbf{A}}$ will be denoted by $a_{i,j}$. The vector with all of its elements equal to unity is denoted by $\mathbf{1}$.

Let $\mathbf{x}(m_1, m_2) \in [0, 255]^3$ represent the input RGB image to be halftoned. $\mathbf{X}(z_1, z_2)$ represents the z-transform of the RGB input image

$$\mathbf{X}(z_1, z_2) = \sum_{m_1, m_2} \mathbf{x}(m_1, m_2) z^{-m_1} z^{-m_2}. \tag{1}$$

We will use an index $\mathbf{m}$ to denote a 2-D spatial index (m_1, m_2) and $\mathbf{z}$ to denote the z-domain index (z_1, z_2).

B. Notation for Vector Color Error Diffusion

Fig. 1 shows the system block diagram for vector color error diffusion halftoning. The rendering scalar quantizer is defined by $\mathbf{Q}$: $\mathcal{R}^3 \mapsto \mathcal{U}$ where $\mathcal{U} = \mathcal{U}_1 \times \mathcal{U}_2 \times \mathcal{U}_3$ maps the modified input vector $\mathbf{u}(\mathbf{m})$ into a rendered output vector $\mathbf{b}(\mathbf{m})$. $\mathcal{U}_i$, $i = 1, 2, 3$, represents the alphabet used to represent the ith component of the rendered output. We assume that the output to be restricted to one bit per color plane with 255 representing the presence of a color component and 0 representing the absence of a color component, $\mathcal{U}_i = \{0, 255\}, \ \forall i$. The results of this paper are valid for any equal, uniform bit allocation among the RGB channel quantizers.

The quantization error vector $\mathbf{e}(\mathbf{m})$ is formed by subtracting the quantizer input from the output

$$\mathbf{e}(\mathbf{m}) = \mathbf{b}(\mathbf{m}) - \mathbf{u}(\mathbf{m}). \tag{2}$$

The error vector sequence is then filtered by an error filter $\tilde{\mathbf{h}}(\cdot)$ to produce the feedback signal. The error filter $\tilde{\mathbf{h}}(\cdot)$ is a filter with matrix-valued coefficients and will be denoted by the 3×3 matrix-valued sequence $\tilde{\mathbf{h}}(\cdot)$ with support set $\mathcal{S}$. $\tilde{\mathbf{H}}(\cdot)$ represents the z-transform of the matrix-valued multifilter defined by

$$\tilde{\mathbf{H}}(z_1, z_2) = \sum_{m_1, m_2} \tilde{\mathbf{h}}(m_1, m_2) z^{-m_1} z^{-m_2}. \tag{3}$$

The filtering operation of a 2-D multifilter is defined by matrix-vector convolution given by

$$\left[\tilde{\mathbf{h}} \star \mathbf{e}\right](\mathbf{m}) = \sum_{\mathbf{k} \in \mathcal{S}} \tilde{\mathbf{h}}(\mathbf{k}) \mathbf{e}(\mathbf{m} - \mathbf{k}). \tag{4}$$

Here the error filter is assumed to have causal support $\mathcal{S}$ with $(0, 0) \notin \mathcal{S}$. We will assume the standard four-coefficient Floyd–Steinberg filter [6] support set. In the z domain, the matrix-vector convolution becomes a linear transformation by an 3×3 transformation matrix given by

$$Z\left[\tilde{\mathbf{h}} \star \mathbf{e}\right](\mathbf{z}) = \tilde{\mathbf{H}}(\mathbf{z}) \mathbf{E}(\mathbf{z}). \tag{5}$$

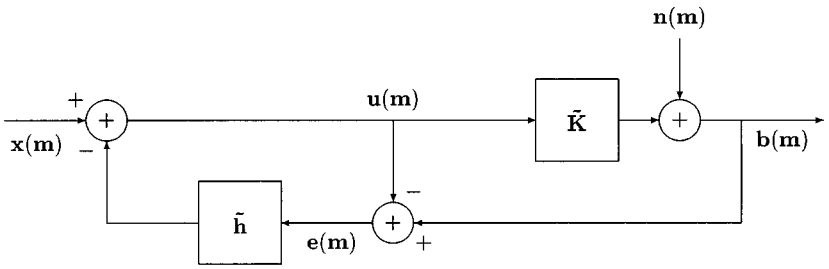

Fig. 2. System block diagram for vector color error diffusion model, where $\bar{\mathbf{K}}$ represents a linear transformation of the signal component $\mathbf{u}(\mathbf{m})$ and $\mathbf{n}(\mathbf{m})$ is a noise process uncorrelated with the signal component of $\mathbf{u}(\mathbf{m})$.

The modified input is computed by subtracting the feedback signal from the input signal

$$\mathbf{u}(\mathbf{m}) = \mathbf{x}(\mathbf{m}) - \left[\tilde{\mathbf{h}} \star \mathbf{e}\right](\mathbf{m}). \tag{6}$$

III. Matrix Gain Model for Vector Color Error Diffusion

This section generalizes the linear system model of grayscale error diffusion in [3] to vector color error diffusion by replacing the "linear gain model" with a new "matrix gain model" and using properties of filters with matrix-valued coefficients discussed in Section II. The new model includes the earlier model [3], [7] as a special case. The new model describes vector color diffusion in the frequency domain, and predicts noise shaping and linear frequency distortion produced by error diffusion halftoning. For vector color halftoning, we also derive the necessary and sufficient condition for linear distortion elimination via prefiltering.

Section III-A describes how vector error diffusion may be linearized via the proposed matrix gain model. Signal and noise shaping transfer functions are derived based on an analysis of the linearized system. Section III-B validates the predictions of the matrix gain model by halftoning test images. We show that a linear shift-invariant prefilter can eliminate the linear signal frequency-distortion effects of error diffusion. Further, we show that such a pre-filter can be incorporated with low-complexity by modifying the error diffusion system to feed a linear transformation of the quantizer input. Section III-C considers the mathematical validity of the modeling and comments on the invertibility of certain matrices used in the matrix gain model.

A. Linearizing Vector Color Error Diffusion

We model the quantizer of Fig. 1 by a constant linear transformation denoted by a matrix $\tilde{\mathbf{K}}$ which is applied to the signal components of the quantizer input plus spatially-varying additive noise $\mathbf{n}(\mathbf{m})$ applied to the noise components (components uncorrelated with the input signal) of the quantizer input, as shown in Fig. 2. This is a generalization of modeling the quantizers in sigma–delta modulators [8] and grayscale error diffusion [3], [7]. Correlation among the signal color planes is represented by the off-diagonal terms in the matrix $\tilde{\mathbf{K}}$. We choose the matrix $\tilde{\mathbf{K}}$ to minimize the error in approximating the quantizer with a linear transformation, in the linear minimum mean squared error (LMMSE) sense

$$\tilde{\mathbf{K}} = \arg\min_{\tilde{\mathbf{A}}} E\left[\|\mathbf{b}(\mathbf{m}) - \tilde{\mathbf{A}}\,\mathbf{u}(\mathbf{m})\|^2\right] \tag{7}$$

where $\mathbf{b}(\cdot)$ represents the quantizer output process, and $\mathbf{u}(\cdot)$ represents the quantizer input process. The solution to (7) when $\mathbf{b}(\cdot)$ and $\mathbf{u}(\cdot)$ are wide sense stationary processes is [15]

$$\tilde{\mathbf{K}} = \tilde{\mathbf{C}}_{\mathbf{bu}}\tilde{\mathbf{C}}_{\mathbf{uu}}^{-1} \tag{8}$$

where $\tilde{\mathbf{C}}_{\mathbf{bu}}$ and $\tilde{\mathbf{C}}_{\mathbf{uu}}$ are covariance matrices. As a direct consequence of this modeling [15], the noise process $\mathbf{n}(\cdot)$ due to the signal approximation error is uncorrelated with the signal input to the quantizer $\mathbf{u}(\cdot)$. We will analyze error diffusion by assuming a matrix gain of $\tilde{\mathbf{K}}$ for the signal path and a matrix gain of $\tilde{\mathbf{I}}$ (identity matrix) for the noise path. This corresponds to using the estimator to estimate signal components in the output of the quantizer from signal components at its input, and assuming an uncorrelated noise injection to model the noise. In this way, one may treat the signal shaping and noise shaping independently. This is similar to the analysis for grayscale error diffusion in [3], [7].

Analyzing the linearized vector color error diffusion model of Fig. 2 in the frequency domain using z-transforms yields

$$Z\left[\tilde{\mathbf{h}} \star \mathbf{e}\right](\mathbf{z}) = \tilde{\mathbf{H}}(\mathbf{z})\mathbf{E}(\mathbf{z}). \tag{9}$$

By analyzing the signal path and ignoring the noise path by setting $\mathbf{n}(\mathbf{m}) = \mathbf{0}$

$$\mathbf{X}(\mathbf{z}) = \mathbf{U}(\mathbf{z}) + \tilde{\mathbf{H}}(\mathbf{z})\mathbf{E}(\mathbf{z}) \tag{10}$$

$$\mathbf{E}(\mathbf{z}) = (\tilde{\mathbf{K}} - \tilde{\mathbf{I}})\mathbf{U}(\mathbf{z}) \tag{11}$$

$$\mathbf{B}_s(\mathbf{z}) = \tilde{\mathbf{K}}\mathbf{U}(\mathbf{z}). \tag{12}$$

By manipulating (10)–(12), the response to the signal component becomes

$$\mathbf{B}_s(\mathbf{z}) = \tilde{\mathbf{K}}\left[\tilde{\mathbf{I}} + \tilde{\mathbf{H}}(\mathbf{z})\,(\tilde{\mathbf{K}} - \tilde{\mathbf{I}})\right]^{-1}\mathbf{X}(\mathbf{z}). \tag{13}$$

By considering the contribution of the noise component $\mathbf{B}(\mathbf{z})$ to the output $\mathbf{B}_n(\mathbf{z})$

$$\mathbf{B}_n(\mathbf{z}) = \mathbf{N}(\mathbf{z}) + \mathbf{U}(\mathbf{z}) \tag{14}$$

$$\mathbf{U}(\mathbf{z}) = -\tilde{\mathbf{H}}(\mathbf{z})\mathbf{E}(\mathbf{z}) \tag{15}$$

$$\mathbf{E}(\mathbf{z}) = \mathbf{N}(\mathbf{z}). \tag{16}$$

(a) (b)

(c) (d)

Fig. 3. Validation of matrix gain model by linearly distorting the original image. Here, the residual image has been scaled using a full-scale contrast stretch for display purposes.

By rearranging (14)–(16),

$$\mathbf{B}_n(\mathbf{z}) = \left[\tilde{\mathbf{I}} - \tilde{\mathbf{H}}(\mathbf{z})\right] \mathbf{N}(\mathbf{z}). \tag{17}$$

The overall system response is given by

$$\mathbf{B}(\mathbf{z}) = \mathbf{B}_s(\mathbf{z}) + \mathbf{B}_n(\mathbf{z}). \tag{18}$$

Equations (13) and (17) reduce to the analogous ones for grayscale error diffusion [3], in which the error filter coefficients and signal gain are scalar valued. The next section validates the analysis given in this section, and shows that it accurately models the linear distortion and noise shaping of vector color error diffusion.

B. Validating the Matrix Gain Model

This section validates the matrix gain model by using it to predict the linear distortion and noise shaping effects of vector color error diffusion. Section III-B1 shows that the signal path distortion given by (13) accurately models the linear distortion to which the original color image is subjected in vector color error diffusion. Section III-B2 shows that by adding a specified linear transformation of the input image to the quantizer input, the linear distortion may be eliminated. Thus, the modeling predicts that a flat frequency response can be achieved. This will be validated through simulation. Section III-B3 validates that the model accurately predicts the noise shaping behavior of vector color error diffusion. In the validation process, we use a fixed matrix-valued error filter whose coefficients were obtained by terminating the adaptive algorithm of [10] after a fixed number of iterations. The results hold for an arbitrary fixed set of matrix-valued filter coefficients, and hence, there is no loss of generality.

1) Validation by Constructing a Linearly Distorted Original: We linearly distort the original image without introducing quantization noise by processing the original image of Fig. 3(a) by using (13). This is equivalent to processing the original image according to Fig. 2, with the additive noise ignored. Fig. 3(b) shows the resulting image. Fig. 3(c) shows the result of halftoning with the fixed error filter. Fig. 3(b) and (c) have comparable linear distortion. To see this, we simply form

the residual image by subtracting Fig. 3(b) from Fig. 3(c). The result is shown in Fig. 3(d). The residual in Fig. 3(d) is uncorrelated with the original and represents quantization noise. This is consistent with the modeling of Section III-A. To quantify the degree of correlation of the residual image with the original image, we introduce a correlation matrix defined by

$$\tilde{\mathbf{C}}_{\mathbf{rx}} = \begin{pmatrix} \rho_{r_{red}x_{red}} & \rho_{r_{red}x_{green}} & \rho_{r_{red}x_{blue}} \\ \rho_{r_{green}x_{red}} & \rho_{r_{green}x_{green}} & \rho_{r_{green}x_{blue}} \\ \rho_{r_{blue}x_{red}} & \rho_{r_{blue}x_{green}} & \rho_{r_{blue}x_{blue}} \end{pmatrix} \quad (19)$$

where $\rho_{r_i x_j}$ represents the correlation coefficient [15] between the color plane i in the residual and the color plane j in the original image. The correlation matrix for the residual shown in Fig. 3(d), with respect to the original image shown in Fig. 3(a), is

$$\tilde{\mathbf{C}}_{\mathbf{rx}} = \begin{pmatrix} 0.0067 & 0.0007 & 0.0051 \\ 0.0065 & 0.0039 & 0.0049 \\ 0.0082 & 0.0040 & 0.0062 \end{pmatrix}.$$

2) Validation by Constructing an Undistorted Halftone: The model predicts that the linear distortion suffered by the color input image is given by (13). This means that if one prefilters the input color image by using the filter

$$\tilde{\mathbf{G}}(\mathbf{z}) = \left[\tilde{\mathbf{I}} + \tilde{\mathbf{H}}(\mathbf{z})(\tilde{\mathbf{K}} - \tilde{\mathbf{I}})\right]\tilde{\mathbf{K}}^{-1} \quad (20)$$

then the resulting halftone should exhibit a flat low-frequency response with respect to the original color image. Fig. 4 shows error diffusion modified to include the prefilter. We now prove the following proposition.

Proposition 1: Fig. 4 is exactly equivalent to Fig. 5 when $\tilde{\mathbf{L}} = \tilde{\mathbf{K}}^{-1} - \tilde{\mathbf{I}}$, whenever $[\tilde{\mathbf{I}} - \tilde{\mathbf{H}}(\mathbf{z})]$ is invertible.

Proof: By analyzing Fig. 4, the input to the quantizer $\mathbf{u(m)}$ in the z-domain is

$$\mathbf{U}(\mathbf{z}) = \tilde{\mathbf{G}}(\mathbf{z})\mathbf{X}(\mathbf{z}) - \tilde{\mathbf{H}}(\mathbf{z})\mathbf{E}(\mathbf{z}) \quad (21)$$

$$\mathbf{E}(\mathbf{z}) = \mathbf{B}(\mathbf{z}) - \mathbf{U}(\mathbf{z}). \quad (22)$$

From (21) and (22)

$$\mathbf{E}(\mathbf{z}) = \left[\tilde{\mathbf{I}} - \tilde{\mathbf{H}}(\mathbf{z})\right]^{-1}\left[\mathbf{B}(\mathbf{z}) - \tilde{\mathbf{G}}(\mathbf{z})\mathbf{X}(\mathbf{z})\right]. \quad (23)$$

Substituting for $\mathbf{E}(\mathbf{z})$ given by (23) in (21) yields

$$\mathbf{U}(\mathbf{z}) = \left[\tilde{\mathbf{I}} + \tilde{\mathbf{H}}(\mathbf{z})\left(\tilde{\mathbf{I}} - \tilde{\mathbf{H}}(\mathbf{z})\right)^{-1}\right]\tilde{\mathbf{G}}(\mathbf{z})\mathbf{X}(\mathbf{z}) - \tilde{\mathbf{H}}(\mathbf{z})\left(\tilde{\mathbf{I}} - \tilde{\mathbf{H}}(\mathbf{z})\right)^{-1}\mathbf{B}(\mathbf{z}). \quad (24)$$

Now, by analyzing Fig. 5

$$\mathbf{U}(\mathbf{z}) = \mathbf{X}(\mathbf{z}) - \tilde{\mathbf{H}}(\mathbf{z})\mathbf{E}(\mathbf{z}) \quad (25)$$

$$\mathbf{E}(\mathbf{z}) = \mathbf{B}(\mathbf{z}) - \mathbf{U}(\mathbf{z}). \quad (26)$$

From (25) and (26)

$$\mathbf{E}(\mathbf{z}) = \left[\tilde{\mathbf{I}} - \tilde{\mathbf{H}}(\mathbf{z})\right]^{-1}[\mathbf{B}(\mathbf{z}) - \mathbf{X}(\mathbf{z})]. \quad (27)$$

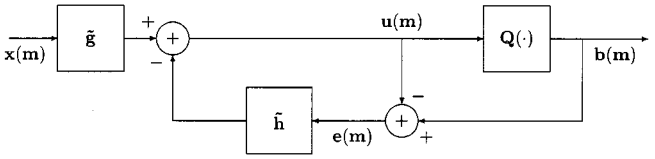

Fig. 4. System block diagrams for vector color error diffusion halftoning with a fixed pre-filter $\tilde{\mathbf{g}}$ having matrix valued coefficients.

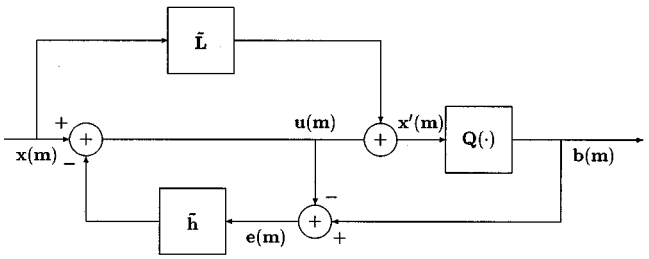

Fig. 5. System block diagram for modified vector color error diffusion halftoning.

Also, since

$$\mathbf{X}'(\mathbf{z}) = \left[\tilde{\mathbf{I}} + \tilde{\mathbf{L}}\right]\mathbf{X}(\mathbf{z}) - \tilde{\mathbf{H}}(\mathbf{z})\mathbf{E}(\mathbf{z}) \quad (28)$$

we substitute (27) into (28)

$$\mathbf{X}'(\mathbf{z}) = \left[(\tilde{\mathbf{I}} + \tilde{\mathbf{L}}) + \tilde{\mathbf{H}}(\mathbf{z})\left[\tilde{\mathbf{I}} - \tilde{\mathbf{H}}(\mathbf{z})\right]^{-1}\right]\mathbf{X}(\mathbf{z}) - \tilde{\mathbf{H}}(\mathbf{z})\left(\tilde{\mathbf{I}} - \tilde{\mathbf{H}}(\mathbf{z})\right)^{-1}\mathbf{B}(\mathbf{z}). \quad (29)$$

Comparing (24) and (29), it follows that Figs. 4 and 5 are equivalent in the sense that they have the same quantizer input and hence output if

$$\left[(\tilde{\mathbf{I}} + \tilde{\mathbf{L}}) + \tilde{\mathbf{H}}(\mathbf{z})\left[\tilde{\mathbf{I}} - \tilde{\mathbf{H}}(\mathbf{z})\right]^{-1}\right] = \left[\tilde{\mathbf{I}} + \tilde{\mathbf{H}}(\mathbf{z})\left(\tilde{\mathbf{I}} - \tilde{\mathbf{H}}(\mathbf{z})\right)^{-1}\right]\tilde{\mathbf{G}}(\mathbf{z}). \quad (30)$$

By using

$$\tilde{\mathbf{P}}(\mathbf{z}) = \tilde{\mathbf{I}} + \tilde{\mathbf{H}}(\mathbf{z})\left(\tilde{\mathbf{I}} - \tilde{\mathbf{H}}(\mathbf{z})\right)^{-1} \quad (31)$$

(30) becomes

$$\tilde{\mathbf{L}} = \tilde{\mathbf{P}}(\mathbf{z})\left[\tilde{\mathbf{G}}(\mathbf{z}) - \tilde{\mathbf{I}}\right]. \quad (32)$$

Substituting for $\tilde{\mathbf{G}}(\mathbf{z})$ given by (20)

$$\begin{aligned}\tilde{\mathbf{L}} &= \tilde{\mathbf{P}}(\mathbf{z})\left[\left[\tilde{\mathbf{I}} + \tilde{\mathbf{H}}(\mathbf{z})(\tilde{\mathbf{K}} - \tilde{\mathbf{I}})\right]\tilde{\mathbf{K}}^{-1} - \tilde{\mathbf{I}}\right] \\ &= \tilde{\mathbf{P}}(\mathbf{z})\left[\tilde{\mathbf{K}}^{-1} + \tilde{\mathbf{H}}(\mathbf{z}) - \tilde{\mathbf{H}}(\mathbf{z})\tilde{\mathbf{K}}^{-1} - \tilde{\mathbf{I}}\right] \\ &= \tilde{\mathbf{P}}(\mathbf{z})\left[\left[\tilde{\mathbf{I}} - \tilde{\mathbf{H}}(\mathbf{z})\right]\left[\tilde{\mathbf{K}}^{-1} - \tilde{\mathbf{I}}\right]\right] = \tilde{\mathbf{K}}^{-1} - \tilde{\mathbf{I}}. \end{aligned} \quad (33)$$

This completes the proof.

For grayscale error diffusion, this result reduces to the result derived in [3] in which the gain is scalar-valued and the error

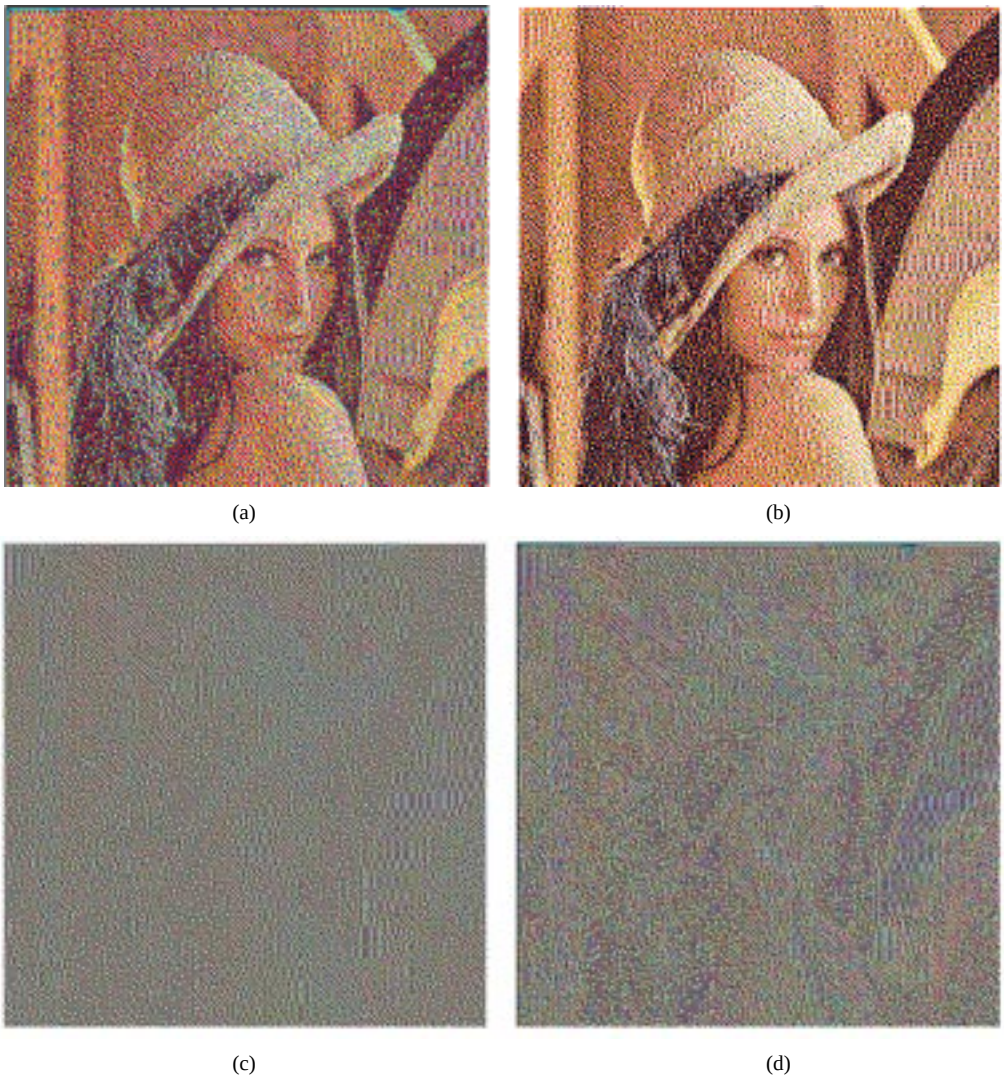

(a) (b) (c) (d)

Fig. 6. Validation of matrix gain model by creating an undistorted halftone. Here, the residual image and the input to the error filter have been scaled using a full-scale contrast stretch for display purposes. (a) Residual image when $\tilde{\mathbf{L}} = \tilde{\mathbf{0}}$. Halftone generated using optimal $\tilde{\mathbf{L}}$. (c) Residual image using optimal $\tilde{\mathbf{L}}$. (d) Input to error filter using optimal $\tilde{\mathbf{L}}$.

filter has scalar coefficients. Fig. 5 feeds a linear transformation $\tilde{\mathbf{L}}$ of the input image into the quantizer input. The matrix gain model predicts that the linear distortion in the halftoning process must be eliminated. To check this result, we first compute the residual of an unmodified halftone (i.e., halftoned using $\tilde{\mathbf{L}} = \tilde{\mathbf{0}}$) with respect to the original. Fig. 3(a) shows the original image to be halftoned. Fig. 3(c) shows the halftone image, which was halftoned with $\tilde{\mathbf{L}} = \tilde{\mathbf{0}}$ (usual vector color error diffusion). Fig. 6(a) shows the residual with respect to the original by subtracting Fig. 3(c) from Fig. 3(a). The correlation matrix for the residual is

$$C_{\mathbf{rx}} = \begin{pmatrix} 0.3204 & 0.2989 & 0.0999 \\ 0.2787 & 0.3295 & 0.1605 \\ 0.2063 & 0.2952 & 0.1836 \end{pmatrix}.$$

Fig. 6(b) shows the halftone image, which was halftoned with $\tilde{\mathbf{L}} = \tilde{\mathbf{K}}^{-1} - \tilde{\mathbf{I}}$ (modified vector color error diffusion). Fig. 6(c) shows the residual with respect to the original by subtracting Fig. 6(b)from Fig. 3(a). The correlation matrix for the residual is

$$\tilde{C}_{\mathbf{rx}} = \begin{pmatrix} 0.0052 & 0.0009 & 0.0040 \\ 0.0054 & 0.0023 & 0.0020 \\ 0.0058 & 0.0011 & 0.0027 \end{pmatrix}.$$

This shows that the linear distortion has been removed by modified vector color error diffusion, since the residual with respect to the original is uncorrelated noise (signal components in the residual have been eliminated).

Knox [2] shows that the error image for grayscale error diffusion $\mathbf{e}(\mathbf{m})$ is correlated with the input image. Knox also shows that the sharpness of halftones increases as the correlation of the error image with the input increases. Kite *et al.* [3] show that by adding dither, the quantization error may be decorrelated with respect to the input, and the sharpening (linear distortion) effects of error diffusion vanish. They also conclude [3] that image sharpening is due to the fact that the input to the error filter contains signal components, which are fed back and shaped. Since the system has a highpass response, this results in the halftone being sharper than the original image.

We will show by using the matrix gain model that in the case of modified error diffusion (Fig. 5), halftoning with the value of $\tilde{\mathbf{L}}$ that cancels linear distortion is a sufficient condition for the error image (input to the error filter) to be free of signal components from the input image.

By replacing the quantizer in Fig. 5 with a gain matrix $\tilde{\mathbf{K}}$ and analyzing the signal path

$$\begin{aligned}\mathbf{E}_s(\mathbf{z}) &= \tilde{\mathbf{K}}\left[\tilde{\mathbf{L}}\mathbf{X}(\mathbf{z}) + \mathbf{U}(\mathbf{z})\right] - \mathbf{U}(\mathbf{z}) \\ &= \tilde{\mathbf{K}}\,\tilde{\mathbf{L}}\,\mathbf{X}(\mathbf{z}) + \left[\tilde{\mathbf{K}} - \tilde{\mathbf{I}}\right]\mathbf{U}(\mathbf{z}). \end{aligned} \tag{34}$$

Since

$$\mathbf{U}(\mathbf{z}) = \mathbf{X}(\mathbf{z}) - \tilde{\mathbf{H}}(\mathbf{z})\,\mathbf{E}_s(\mathbf{z}) \tag{35}$$

we obtain

$$\left[\tilde{\mathbf{I}} + \left(\tilde{\mathbf{K}} - \tilde{\mathbf{I}}\right)\tilde{\mathbf{H}}(\mathbf{z})\right]\mathbf{E}_s(\mathbf{z}) = \left[\tilde{\mathbf{K}}\,\tilde{\mathbf{L}} + \tilde{\mathbf{K}} - \tilde{\mathbf{I}}\right]\mathbf{X}(\mathbf{z}). \tag{36}$$

By substituting $\tilde{\mathbf{L}} = \tilde{\mathbf{K}}^{-1} - \tilde{\mathbf{I}}$ into (36), $\mathbf{E}_s(\mathbf{z}) = 0$. Hence, there are no signal components in the error image. To check this prediction, and hence validate our modeling, we halftone test images with $\tilde{\mathbf{L}}$ set to cancel linear distortion. Fig. 3(a) shows the original image to be halftoned. Fig. 6(b) shows the halftone image by halftoning with $\tilde{\mathbf{L}} = \tilde{\mathbf{K}}^{-1} - \tilde{\mathbf{I}}$ (modified vector color error diffusion). Fig. 6(d) shows the error image. The correlation matrix for the error image with respect to the original is

$$\tilde{C}_{\mathbf{ex}} = \begin{pmatrix} 0.0455 & 0.0235 & 0.0122 \\ 0.0493 & 0.0144 & 0.0164 \\ 0.0428 & 0.0142 & 0.0150 \end{pmatrix}.$$

The low correlation of the error image was predicted by the theory and therefore strongly corroborates it.

3) Validation of the Noise Response: According to our model, the noise shaping is predicted by (17). To verify the prediction, we first compute a residual as described in Section III-B1. This residual is shaped noise. We need to verify that the noise shaping is in fact given by (17). We halftone test images using the optimal linear distortion cancelling method described in Section III-B2. This corresponds to halftoning with the value of $\tilde{\mathbf{L}} = \tilde{\mathbf{K}}^{-1} - \tilde{\mathbf{I}}$. The matrix gain model predicts that the input to the error filter has no signal components. The input to the error filter in this case is $\mathbf{N}(\mathbf{z})$. We then filter this noise image (i.e., input to the error filter) according to (17) to form a predicted residual. If the noise shaping equation is correct, then this residual must be spectrally close to the actual residual image. This was indeed found to be the case. Fig. 7 shows radially averaged spectra of the three color planes of the actual residual noise image and the residual computed using the noise shaping predicted from the model. The close agreement of the spectra confirms the predictions of the matrix gain model. The next section analyzes the valid use of the matrix gain model by considering the existence of matrix inverses assumed by the model.

C. Invertibility of Matrices Used in the Model

Typically, the matrix $\tilde{\mathbf{K}}$ is diagonally dominant with its diagonal elements greater than 1, so it is invertible. For the same reason, the matrix $[\tilde{\mathbf{I}} + \tilde{\mathbf{H}}(\mathbf{z})(\tilde{\mathbf{K}} - \tilde{\mathbf{I}})]$ in (13) is typically invertible. The proof of *Proposition 1* requires that the matrix $[\tilde{\mathbf{I}} - \tilde{\mathbf{H}}(\mathbf{z})]$ be invertible. This is typically not satisfied at DC for filters like the Floyd–Steinberg filter because $[\tilde{\mathbf{I}} - \tilde{\mathbf{H}}(\mathbf{1})] = \tilde{\mathbf{0}}$. However, empirical results indicate that $\lim_{\mathbf{z}\to\mathbf{1}} \mathbf{E}(\mathbf{z})$ does not blow up [16] because $\mathbf{B}(\mathbf{1}) \approx \mathbf{X}(\mathbf{1})$ and $\tilde{\mathbf{G}}(\mathbf{1}) = \tilde{\mathbf{I}}$. In fact, the zero at DC cancels the pole at DC, and $\lim_{\mathbf{z}\to\mathbf{1}} \mathbf{E}(\mathbf{z}) = \mathbf{0}$ for the block diagram of Fig. 5 and equals $-\tilde{\mathbf{L}}\mathbf{X}(\mathbf{1})$ for the block-diagram of Fig. 4. This means that the two block diagrams are equivalent at DC because they have the same input to the quantizer. This is predicted by the matrix gain model. Consider Fig. 5 by noting that

$$\begin{aligned}\left[\tilde{\mathbf{I}} - \tilde{\mathbf{H}}(\mathbf{z})\right]\mathbf{E}(\mathbf{z}) &= \mathbf{B}(\mathbf{z}) - \mathbf{X}(\mathbf{z}) \\ &= \tilde{\mathbf{K}}\left[\tilde{\mathbf{I}} + \tilde{\mathbf{L}}\right]\mathbf{X}(\mathbf{z}) - \tilde{\mathbf{K}}\tilde{\mathbf{H}}(\mathbf{z})\mathbf{E}(\mathbf{z}). \end{aligned} \tag{37}$$

This implies that

$$\left[\tilde{\mathbf{I}} - \tilde{\mathbf{H}}(\mathbf{z}) + \tilde{\mathbf{K}}\tilde{\mathbf{H}}(\mathbf{z})\right]\mathbf{E}(\mathbf{z}) = \left[\tilde{\mathbf{K}}(\tilde{\mathbf{I}} + \tilde{\mathbf{L}}) - \tilde{\mathbf{I}}\right]\mathbf{X}(\mathbf{z}). \tag{38}$$

By taking the limit as $\mathbf{z} \to \mathbf{1}$

$$\mathbf{E}(\mathbf{1}) = \left[\tilde{\mathbf{I}} + \tilde{\mathbf{L}} - \tilde{\mathbf{K}}^{-1}\right]\mathbf{X}(\mathbf{1}) = \mathbf{0}. \tag{39}$$

By analyzing Fig. 4 in a similar manner, $\lim_{\mathbf{z}\to\mathbf{1}} = -\tilde{\mathbf{L}}\,\mathbf{X}(\mathbf{1})$.

From (21) and (28), the two block-diagrams are equivalent at DC. At other frequencies for which $[\tilde{\mathbf{I}} - \tilde{\mathbf{H}}(\mathbf{z})]$ might not be invertible, a similar analysis using the matrix gain model may be applied to show that Figs. 4 and 5 are equivalent. However, the *exact* analysis may be in error to some extent when $[\tilde{\mathbf{I}} - \tilde{\mathbf{H}}(\mathbf{z})]$ is not invertible.

IV. Designing the Error Filter

In designing the color error filter coefficients, we use the matrix gain model along with a sophisticated model for human color vision. The formulation results in an uncorrelated noise image replacing the highly correlated error image in the objective function of [12]. Thus, the optimization becomes less restrictive since we do not compensate for or try to minimize correlated signal components in the error image. Recall from Section III that the correlated signal components in the error image produced a sharpening effect which is usually desirable. We assume the *uncorrelated* noise image is a white noise process as in [11]. We minimize the visual impact of the quantization noise by incorporating the matrix gain model into the optimization along with a linear model for human color vision. We show that the optimal filter may be obtained by a solution of a matrix version of the Yule–Walker equations [17]. Because the error filter does not need to minimize correlated signal components, the filter can be solely optimized for optimal noise shaping.

Section IV-A formulates the design problem as a quadratic optimization problem with linear constraints. Section IV-B derives

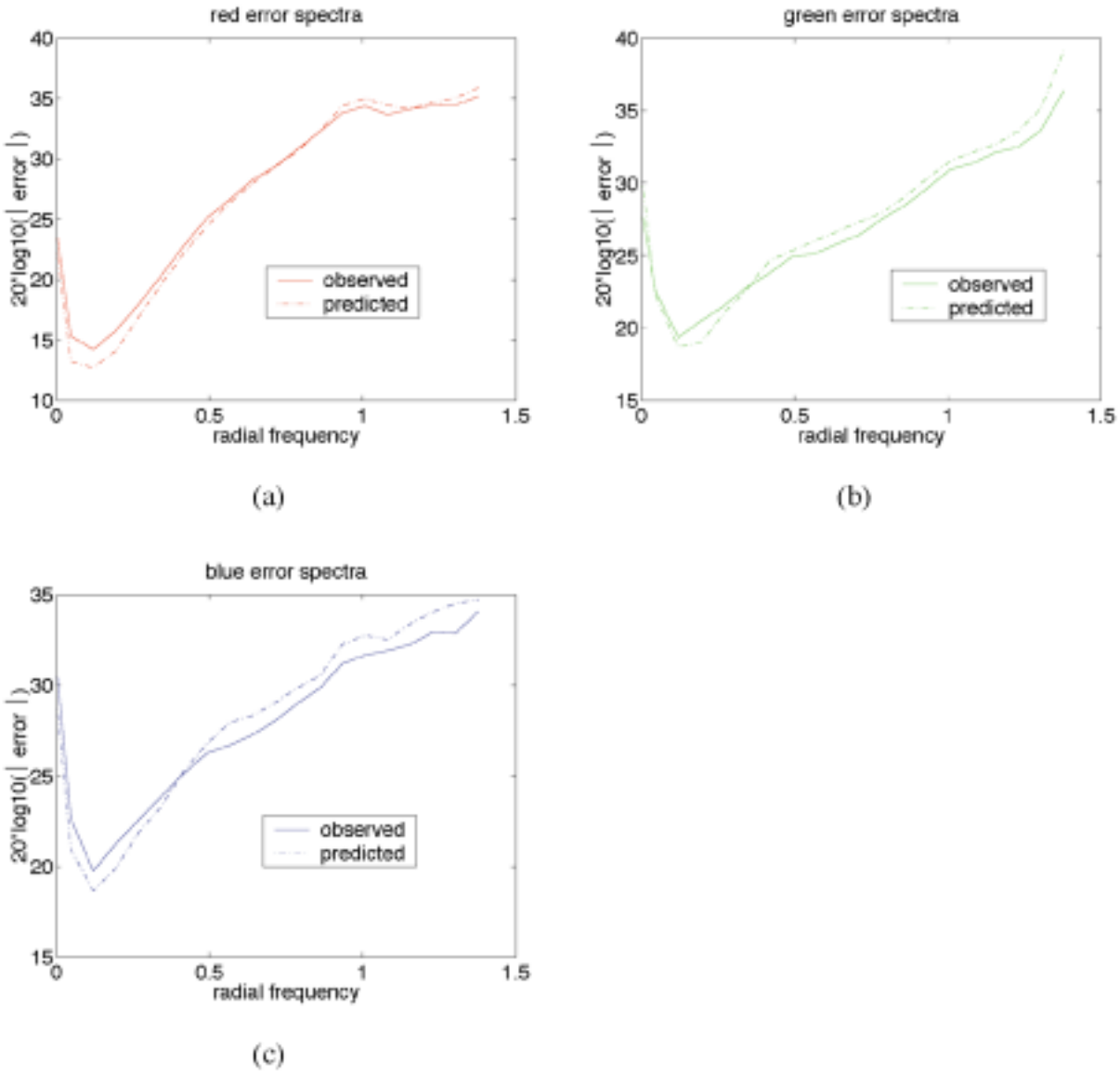

Fig. 7. Predicted and actual spectra for residual noise image: (a) and (b) green and (c) blue planes. Solid lines indicate actual spectra while the dashed lines represent predicted spectra.

the optimal solution and uses a gradient-descent algorithm to compute the optimal filter coefficients. Section IV-C describes a linear color model for the human visual system and shows that it may be represented as a linear transformation followed by spatial filtering. Our solution, however, allows for any general linear shift-invariant color vision model to be used. In Section IV-D, the optimal solution is compared quantitatively and qualitatively to separable Floyd–Steinberg error diffusion.

A. Formulation of the Design Problem

We use the matrix gain model to predict the noise shaping behavior of the color error diffusion system. Based on the matrix gain model, we obtain the net noise component of the output as

$$\mathbf{b}_n(\mathbf{m}) = \left(\left[\tilde{\mathbf{I}} - \tilde{\mathbf{h}}\right] \star \mathbf{n}\right)(\mathbf{m}). \tag{40}$$

Since signal shaping is typically desirable or in any case under user control [18] we only need to concentrate on the noise shaping. We define the objective function J as the average visually weighted noise energy in the output halftone. We use a linear spatially invariant matrix-valued model for the human visual system denoted by the matrix-valued filter function $\tilde{\mathbf{v}}(\cdot)$. We also define a constraint set $\mathcal{C}$ to ensure that all the quantization error (represented in a device independent RGB space) is diffused [18].

Thus, the color error diffusion system $(\tilde{\mathbf{h}}(\cdot), \tilde{\mathbf{v}}(\cdot))$ for a given vision model $\tilde{\mathbf{v}}(\cdot)$ may be solved for an optimum filter $\tilde{\mathbf{h}}_{opt}(\cdot)$

$$\tilde{\mathbf{h}}_{opt}(\cdot) = \arg \min_{\tilde{\mathbf{h}}(\cdot) \in \mathcal{C}} J \tag{41}$$

where

$$J = E\left[\left\|\left(\tilde{\mathbf{v}} \star \left[\tilde{\mathbf{I}} - \tilde{\mathbf{h}}\right] \star \mathbf{n}\right)(\mathbf{m})\right\|^2\right] \tag{42}$$

and

$$\mathcal{C} = \left\{\tilde{\mathbf{h}}(\mathbf{i}),\, \mathbf{i} \in \mathcal{S} \,\middle|\, \sum_{\mathbf{i}} \tilde{\mathbf{h}}(\mathbf{i})\mathbf{1} = \mathbf{1}\right\}. \tag{43}$$

B. Optimum Error Filter Design

The objective function of (42) may be rewritten as

$$J = E\left[\left\|\tilde{\mathbf{a}}(\mathbf{m}) - \left(\tilde{\mathbf{v}} \star \tilde{\mathbf{h}} \star \mathbf{n}\right)(\mathbf{m})\right\|^2\right]$$

$$= E\left[\left\|\tilde{\mathbf{a}}(\mathbf{m}) - \sum_{\mathbf{k}}\sum_{\mathbf{k}'} \tilde{\mathbf{v}}(\mathbf{k}')\tilde{\mathbf{h}}(\mathbf{k})\mathbf{n}(\mathbf{m}-\mathbf{k}'-\mathbf{k})\right\|^2\right]$$

$$= E\,\mathrm{Tr}\left[\tilde{\mathbf{a}}(\mathbf{m}) - \sum_{\mathbf{k}}\sum_{\mathbf{k}'} \tilde{\mathbf{v}}(\mathbf{k}')\tilde{\mathbf{h}}(\mathbf{k})\mathbf{n}(\mathbf{m}-\mathbf{k}'-\mathbf{k})\right] \cdot \left[\tilde{\mathbf{a}}(\mathbf{m}) - \sum_{\mathbf{k}}\sum_{\mathbf{k}'} \tilde{\mathbf{v}}(\mathbf{k}')\tilde{\mathbf{h}}(\mathbf{k})\mathbf{n}(\mathbf{m}-\mathbf{k}'-\mathbf{k})\right]^T \quad (44)$$

where we have substituted $\mathbf{a}(\mathbf{m}) = (\tilde{\mathbf{v}} \star \mathbf{n})(\mathbf{m})$ and used the fact that for a vector $\mathbf{x}$, $\|\mathbf{x}\|^2 = \mathrm{Tr}[\mathbf{x}\mathbf{x}^T]$, where Tr denotes the trace operation. Also since the trace is a linear functional, (44) may be further simplified as

$$J = \Theta_1 + \Theta_2 + \Theta_3 + \Theta_4 \quad (45)$$

where

$$\Theta_1 = E\,\mathrm{Tr}\left[\tilde{\mathbf{a}}(\mathbf{m})\tilde{\mathbf{a}}^T(\mathbf{m})\right] \quad (46)$$

$$\Theta_2 = -E\,\mathrm{Tr}\left[\tilde{\mathbf{a}}(\mathbf{m}) \sum_{\mathbf{k}}\sum_{\mathbf{k}'} \mathbf{n}^T(\mathbf{m}-\mathbf{k}'-\mathbf{k}) \cdot \tilde{\mathbf{h}}^T(\mathbf{k})\tilde{\mathbf{v}}^T(\mathbf{k}')\right] \quad (47)$$

$$\Theta_3 = -E\,\mathrm{Tr}\left[\sum_{\mathbf{k}}\sum_{\mathbf{k}'} \tilde{\mathbf{v}}(\mathbf{k}')\tilde{\mathbf{h}}(\mathbf{k})\mathbf{n}(\mathbf{m}-\mathbf{k}'-\mathbf{k})\tilde{\mathbf{a}}^T(\mathbf{m})\right] \quad (48)$$

$$\Theta_4 = E\,\mathrm{Tr}\left[\sum_{\mathbf{p}}\sum_{\mathbf{q}}\sum_{\mathbf{r}}\sum_{\mathbf{s}} \tilde{\mathbf{v}}(\mathbf{s})\tilde{\mathbf{h}}(\mathbf{r})\mathbf{n}(\mathbf{m}-\mathbf{s}-\mathbf{r}) \cdot \mathbf{n}^T(\mathbf{m}-\mathbf{p}-\mathbf{q})\tilde{\mathbf{h}}^T(\mathbf{p})\tilde{\mathbf{v}}^T(\mathbf{q})\right]. \quad (49)$$

By taking the first partial derivatives of (45) with respect to $\tilde{\mathbf{h}}(\mathbf{i})$ for all $\mathbf{i} \in \mathcal{S}$ and setting them to zero, we obtain the first-order necessary conditions for an optimum solution. This requires that a scalar function be differentiated with respect to a matrix. To do this, some results from linear algebra are required.

The following results are stated here without proof. For proofs of the following, see [17]:

$$\frac{d}{d\tilde{\mathbf{X}}^T} f(\tilde{\mathbf{X}}) = \left(\frac{d}{d\tilde{\mathbf{X}}} f(\tilde{\mathbf{X}})\right)^T \quad (50)$$

$$\frac{d}{d\tilde{\mathbf{X}}}\,\mathrm{Tr}\left(\tilde{\mathbf{A}}\tilde{\mathbf{X}}\right) = \tilde{\mathbf{A}}^T \quad (51)$$

$$\frac{d}{d\tilde{\mathbf{X}}}\,\mathrm{Tr}\left(\tilde{\mathbf{A}}\tilde{\mathbf{X}}\tilde{\mathbf{B}}\right) = \tilde{\mathbf{A}}^T\tilde{\mathbf{B}}^T \quad (52)$$

$$\frac{d}{d\tilde{\mathbf{X}}}\,\mathrm{Tr}\left(\tilde{\mathbf{X}}^T\tilde{\mathbf{A}}\tilde{\mathbf{X}}\tilde{\mathbf{B}}\right) = \tilde{\mathbf{A}}\tilde{\mathbf{X}}\tilde{\mathbf{B}} + \tilde{\mathbf{A}}^T\tilde{\mathbf{X}}\tilde{\mathbf{B}}^T \quad (53)$$

$$\mathrm{Tr}\left(\tilde{\mathbf{A}}\tilde{\mathbf{B}}\right) = \mathrm{Tr}\left(\tilde{\mathbf{B}}\tilde{\mathbf{A}}\right). \quad (54)$$

Let us consider the terms Θ_1, Θ_2, Θ_3 and Θ_4

$$\frac{\partial}{\partial\tilde{\mathbf{h}}(\mathbf{i})}\Theta_1 = 0. \quad (55)$$

By using (50) and (52)

$$\frac{\partial}{\partial\tilde{\mathbf{h}}(\mathbf{i})}\Theta_2 = \left(\frac{\partial}{\partial\tilde{\mathbf{h}}^T(\mathbf{i})}\Theta_2\right)^T$$

$$= -E\left[\frac{d}{d\tilde{\mathbf{h}}^T(\mathbf{i})}\,\mathrm{Tr}\sum_{\mathbf{k}'}\mathbf{a}(\mathbf{m})\mathbf{n}^T(\mathbf{m}-\mathbf{k}'-\mathbf{i}) \cdot \tilde{\mathbf{h}}^T(\mathbf{i})\tilde{\mathbf{v}}^T(\mathbf{k}')\right]^T$$

$$= -E\left[\sum_{\mathbf{k}'}\mathbf{n}(\mathbf{m}-\mathbf{k}'-\mathbf{i})\mathbf{a}^T(\mathbf{m})\tilde{\mathbf{v}}(\mathbf{k}')\right]^T$$

$$= -E\left[\sum_{\mathbf{k}'}\tilde{\mathbf{v}}^T(\mathbf{k}')\mathbf{a}(\mathbf{m})\mathbf{n}^T(\mathbf{m}-\mathbf{k}'-\mathbf{i})\right]$$

$$= -\sum_{\mathbf{k}}\tilde{\mathbf{v}}^T(\mathbf{k})\tilde{\mathbf{r}}_{\mathbf{an}}(-\mathbf{i}-\mathbf{k}). \quad (56)$$

By using (52)

$$\frac{\partial}{\partial\tilde{\mathbf{h}}(\mathbf{i})}\Theta_3$$

$$= -E\left[\frac{\partial}{\partial\tilde{\mathbf{h}}(\mathbf{i})}\,\mathrm{Tr}\sum_{\mathbf{k}'}\tilde{\mathbf{v}}(\mathbf{k}')\tilde{\mathbf{h}}(\mathbf{i})\mathbf{n}(\mathbf{m}-\mathbf{k}'-\mathbf{i})\mathbf{a}^T(\mathbf{m})\right]$$

$$= -E\left[\sum_{\mathbf{k}'}\tilde{\mathbf{v}}^T(\mathbf{k}')\mathbf{a}(\mathbf{m})\mathbf{n}^T(\mathbf{m}-\mathbf{k}'-\mathbf{i})\right]$$

$$= -\sum_{\mathbf{k}}\tilde{\mathbf{v}}^T(\mathbf{k})\tilde{\mathbf{r}}_{\mathbf{an}}(-\mathbf{i}-\mathbf{k}). \quad (57)$$

By considering Θ_4, $\tilde{\mathbf{h}}(\mathbf{i})$ only occurs in three terms Θ_{41}, Θ_{42} and Θ_{43} where

$$\Theta_{41} = E\left[\mathrm{Tr}\sum_{\mathbf{p}\neq\mathbf{i}}\sum_{\mathbf{q}}\sum_{\mathbf{s}}\tilde{\mathbf{v}}(\mathbf{s})\tilde{\mathbf{h}}(\mathbf{i})\mathbf{n}(\mathbf{m}-\mathbf{s}-\mathbf{i}) \cdot \mathbf{n}^T(\mathbf{m}-\mathbf{p}-\mathbf{q})\tilde{\mathbf{h}}^T(\mathbf{p})\tilde{\mathbf{v}}^T(\mathbf{q})\right]$$

$$\Theta_{42} = E\left[\mathrm{Tr}\sum_{\mathbf{r}\neq\mathbf{i}}\sum_{\mathbf{q}}\sum_{\mathbf{s}}\tilde{\mathbf{v}}(\mathbf{s})\tilde{\mathbf{h}}(\mathbf{r})\mathbf{n}(\mathbf{m}-\mathbf{s}-\mathbf{r}) \cdot \mathbf{n}^T(\mathbf{m}-\mathbf{i}-\mathbf{q})\tilde{\mathbf{h}}^T(\mathbf{i})\tilde{\mathbf{v}}^T(\mathbf{q})\right]$$

$$\Theta_{43} = E\left[\mathrm{Tr}\sum_{\mathbf{q}}\sum_{\mathbf{s}}\tilde{\mathbf{v}}(\mathbf{s})\tilde{\mathbf{h}}(\mathbf{i})\mathbf{n}(\mathbf{m}-\mathbf{s}-\mathbf{i}) \cdot \mathbf{n}^T(\mathbf{m}-\mathbf{i}-\mathbf{q})\tilde{\mathbf{h}}^T(\mathbf{i})\tilde{\mathbf{v}}^T(\mathbf{q})\right]. \quad (58)$$

By using (52)

$$\begin{aligned}\frac{\partial}{\partial\tilde{\mathbf{h}}(\mathbf{i})}\Theta_{41} &= E\left[\sum_{\mathbf{p}\neq\mathbf{i}}\sum_{\mathbf{q}}\sum_{\mathbf{s}}\tilde{\mathbf{v}}^T(\mathbf{s})\left\{\mathbf{n}(\mathbf{m}-\mathbf{s}-\mathbf{i})\mathbf{n}^T(\mathbf{m}-\mathbf{p}-\mathbf{q})\cdot\tilde{\mathbf{h}}^T(\mathbf{p})\tilde{\mathbf{v}}^T(\mathbf{q})\right\}^T\right]\\ &= E\left[\sum_{\mathbf{p}\neq\mathbf{i}}\sum_{\mathbf{q}}\sum_{\mathbf{s}}\tilde{\mathbf{v}}^T(\mathbf{s})\tilde{\mathbf{v}}(\mathbf{q})\tilde{\mathbf{h}}(\mathbf{p})\mathbf{n}(\mathbf{m}-\mathbf{p}-\mathbf{q})\cdot\mathbf{n}^T(\mathbf{m}-\mathbf{s}-\mathbf{i})\right]\\ &= \sum_{\mathbf{p}\neq\mathbf{i}}\sum_{\mathbf{q}}\sum_{\mathbf{s}}\tilde{\mathbf{v}}^T(\mathbf{s})\tilde{\mathbf{v}}(\mathbf{q})\tilde{\mathbf{h}}(\mathbf{p})\tilde{\mathbf{r}}_{\mathbf{nn}}(\mathbf{p}+\mathbf{q}-\mathbf{s}-\mathbf{i}). \qquad (59)\end{aligned}$$

By using (50) and (52) as in (56)

$$\begin{aligned}\frac{\partial}{\partial\tilde{\mathbf{h}}(\mathbf{i})}\Theta_{42} &= \left[\frac{\partial}{\partial\tilde{\mathbf{h}}^T(\mathbf{i})}\Theta_{42}\right]^T\\ &= E\left[\sum_{\mathbf{r}\neq\mathbf{i}}\sum_{\mathbf{q}}\sum_{\mathbf{s}}\left\{\tilde{\mathbf{v}}(\mathbf{s})\tilde{\mathbf{h}}(\mathbf{r})\mathbf{n}(\mathbf{m}-\mathbf{s}-\mathbf{r})\cdot\mathbf{n}^T(\mathbf{m}-\mathbf{i}-\mathbf{q})\right\}^T\tilde{\mathbf{v}}(\mathbf{q})\right]^T\\ &= E\left[\sum_{\mathbf{r}\neq\mathbf{i}}\sum_{\mathbf{q}}\sum_{\mathbf{s}}\mathbf{n}(\mathbf{m}-\mathbf{i}-\mathbf{q})\mathbf{n}^T(\mathbf{m}-\mathbf{s}-\mathbf{r})\cdot\tilde{\mathbf{h}}^T(\mathbf{r})\tilde{\mathbf{v}}^T(\mathbf{s})\tilde{\mathbf{v}}(\mathbf{q})\right]^T\\ &= E\left[\sum_{\mathbf{r}\neq\mathbf{i}}\sum_{\mathbf{q}}\sum_{\mathbf{s}}\tilde{\mathbf{v}}^T(\mathbf{q})\tilde{\mathbf{v}}(\mathbf{s})\tilde{\mathbf{h}}(\mathbf{r})\mathbf{n}(\mathbf{m}-\mathbf{s}-\mathbf{r})\cdot\mathbf{n}^T(\mathbf{m}-\mathbf{q}-\mathbf{i})\right]\\ &= \sum_{\mathbf{r}\neq\mathbf{i}}\sum_{\mathbf{q}}\sum_{\mathbf{s}}\tilde{\mathbf{v}}^T(\mathbf{q})\tilde{\mathbf{v}}(\mathbf{s})\tilde{\mathbf{h}}(\mathbf{r})\tilde{\mathbf{r}}_{\mathbf{nn}}(\mathbf{r}+\mathbf{s}-\mathbf{q}-\mathbf{i})\\ &= \sum_{\mathbf{p}\neq\mathbf{i}}\sum_{\mathbf{q}}\sum_{\mathbf{s}}\tilde{\mathbf{v}}^T(\mathbf{s})\tilde{\mathbf{v}}(\mathbf{q})\tilde{\mathbf{h}}(\mathbf{p})\tilde{\mathbf{r}}_{\mathbf{nn}}(\mathbf{p}+\mathbf{q}-\mathbf{s}-\mathbf{i}).\end{aligned} \qquad (60)$$

To simplify $(\partial/\partial\tilde{\mathbf{h}}(\mathbf{i}))\,\Theta_{43}$, we use (54) and (53)

$$\Theta_{43} = E\left[\mathrm{Tr}\sum_{\mathbf{q}}\sum_{\mathbf{s}}\underbrace{\tilde{\mathbf{v}}(\mathbf{s})}_{\tilde{\mathbf{U}}_{\mathbf{s}}}\underbrace{\tilde{\mathbf{h}}(\mathbf{i})}_{\tilde{\mathbf{X}}}\underbrace{\mathbf{n}(\mathbf{m}-\mathbf{s}-\mathbf{i})\mathbf{n}^T(\mathbf{m}-\mathbf{i}-\mathbf{q})}_{\tilde{\mathbf{V}}_{\mathbf{q},\mathbf{s}}}\cdot\underbrace{\tilde{\mathbf{h}}^T(\mathbf{i})}_{\tilde{\mathbf{X}}^T}\underbrace{\tilde{\mathbf{v}}^T(\mathbf{q})}_{\tilde{\mathbf{W}}_{\mathbf{q}}}\right]. \qquad (61)$$

By using (54) in (61) and applying (53)

$$\begin{aligned}\frac{\partial}{\partial\tilde{\mathbf{X}}}\Theta_{43} &= \frac{\partial}{\partial\tilde{\mathbf{X}}}E\left[\mathrm{Tr}\sum_{\mathbf{q}}\sum_{\mathbf{s}}\tilde{\mathbf{U}}_{\mathbf{s}}\tilde{\mathbf{X}}\tilde{\mathbf{V}}_{\mathbf{q},\mathbf{s}}\tilde{\mathbf{X}}^T\tilde{\mathbf{W}}_{\mathbf{q}}\right]\\ &= \frac{\partial}{\partial\tilde{\mathbf{X}}}E\left[\mathrm{Tr}\sum_{\mathbf{q}}\sum_{\mathbf{s}}\tilde{\mathbf{X}}^T\tilde{\mathbf{W}}_{\mathbf{q}}\tilde{\mathbf{U}}_{\mathbf{s}}\tilde{\mathbf{X}}\tilde{\mathbf{V}}_{\mathbf{q},\mathbf{s}}\right]\\ &= E\left[\sum_{\mathbf{q}}\sum_{\mathbf{s}}\tilde{\mathbf{W}}_{\mathbf{q}}\tilde{\mathbf{U}}_{\mathbf{s}}\tilde{\mathbf{X}}\tilde{\mathbf{V}}_{\mathbf{q},\mathbf{s}}+\tilde{\mathbf{U}}_{\mathbf{s}}^T\tilde{\mathbf{W}}_{\mathbf{q}}^T\tilde{\mathbf{X}}\tilde{\mathbf{V}}_{\mathbf{q},\mathbf{s}}^T\right]\\ &= E\left[\sum_{\mathbf{q}}\sum_{\mathbf{s}}\tilde{\mathbf{v}}^T(\mathbf{q})\tilde{\mathbf{v}}(\mathbf{s})\tilde{\mathbf{h}}(\mathbf{i})\mathbf{n}(\mathbf{m}-\mathbf{s}-\mathbf{i})\cdot\mathbf{n}^T(\mathbf{m}-\mathbf{i}-\mathbf{q})\right]\\ &\quad + E\left[\sum_{\mathbf{q}}\sum_{\mathbf{s}}\tilde{\mathbf{v}}^T(\mathbf{s})\tilde{\mathbf{v}}(\mathbf{q})\tilde{\mathbf{h}}(\mathbf{i})\mathbf{n}(\mathbf{m}-\mathbf{i}-\mathbf{q})\cdot\mathbf{n}^T(\mathbf{m}-\mathbf{s}-\mathbf{i})\right]\\ &= 2E\left[\sum_{\mathbf{q}}\sum_{\mathbf{s}}\tilde{\mathbf{v}}^T(\mathbf{s})\tilde{\mathbf{v}}(\mathbf{q})\tilde{\mathbf{h}}(\mathbf{i})\mathbf{n}(\mathbf{m}-\mathbf{i}-\mathbf{q})\cdot\mathbf{n}^T(\mathbf{m}-\mathbf{s}-\mathbf{i})\right]\\ &= 2\sum_{\mathbf{q}}\sum_{\mathbf{s}}\tilde{\mathbf{v}}^T(\mathbf{s})\tilde{\mathbf{v}}(\mathbf{q})\tilde{\mathbf{h}}(\mathbf{i})\tilde{\mathbf{r}}_{\mathbf{nn}}(\mathbf{q}-\mathbf{s}). \qquad (62)\end{aligned}$$

Finally, combining (62) with (60) and (59) and combining (57) and (56) yields the first-order necessary conditions for an optimum solution to the minimization of (42)

$$\begin{aligned}&\sum_{\mathbf{k}}\tilde{\mathbf{v}}^T(\mathbf{k})\tilde{\mathbf{r}}_{\mathbf{an}}(-\mathbf{i}-\mathbf{k})\\ &\quad= \sum_{\mathbf{p}}\sum_{\mathbf{q}}\sum_{\mathbf{s}}\tilde{\mathbf{v}}^T(\mathbf{s})\tilde{\mathbf{v}}(\mathbf{q})\tilde{\mathbf{h}}(\mathbf{p})\tilde{\mathbf{r}}_{\mathbf{nn}}(\mathbf{p}+\mathbf{q}-\mathbf{s}-\mathbf{i}).\end{aligned} \qquad (63)$$

These equations may be regarded as a generalization of the Yule–Walker equations [17] from linear prediction theory to the matrix case, with a generalized linear spatially-invariant weighting. The above set of generalized Yule–Walker equations may be solved for the optimal filter subject to the constraints of (43) using the steepest descent algorithm [17].

We use a white noise image as an approximation to the uncorrelated noise image $\mathbf{n}(\mathbf{m})$. Thus, the required autocorrelation matrices are approximated as

$$\tilde{\mathbf{r}}_{\mathbf{nn}}(\mathbf{k}) = E\left[\mathbf{n}(\mathbf{m})\mathbf{n}^T(\mathbf{m}+\mathbf{k})\right] \approx \delta(\mathbf{k}) \qquad (64)$$

$$\begin{aligned}\tilde{\mathbf{r}}_{\mathbf{an}}(\mathbf{k}) &= E\left(\sum_{\mathbf{t}}\tilde{\mathbf{v}}(\mathbf{t})\mathbf{n}(\mathbf{m}-\mathbf{t})\right)\mathbf{n}^T(\mathbf{m}+\mathbf{k})\\ &\approx \sum_{\mathbf{t}}\tilde{\mathbf{v}}(\mathbf{t})\delta(\mathbf{k}+\mathbf{t}) = \tilde{\mathbf{v}}(-\mathbf{k})\end{aligned} \qquad (65)$$

where $\delta(\mathbf{k})$ is the two-dimensional Kronecker delta function [17]. In the optimization, the constraint is enforced by projection onto the convex constraint set. The convergence behavior of this algorithm is discussed in [19]. The algorithm is guaranteed

to converge if the convergence parameter in the descent algorithm is chosen to be small enough [19].

The descent algorithm may be formulated as

$$\frac{\partial J}{\partial \tilde{\mathbf{h}}^{(\theta)}(\mathbf{i})} \triangleq -2 \sum_{\mathbf{k}} \tilde{\mathbf{v}}^T(\mathbf{k}) \tilde{\mathbf{v}}(\mathbf{i}+\mathbf{k}) + 2 \sum_{\mathbf{p}} \sum_{\mathbf{q}} \sum_{\mathbf{s}} \tilde{\mathbf{v}}^T(\mathbf{s}) \tilde{\mathbf{v}}(\mathbf{q}) \tilde{\mathbf{h}}^{(\theta)}(\mathbf{p}) \delta \cdot (\mathbf{p}+\mathbf{q}-\mathbf{s}-\mathbf{i}) \quad (66)$$

$$\tilde{\mathbf{f}}^{(\theta)}(\mathbf{i}) \triangleq \tilde{\mathbf{h}}^{(\theta)}(\mathbf{i}) - \alpha \frac{\partial J}{\partial \tilde{\mathbf{h}}^{(\theta)}(\mathbf{i})} \quad (67)$$

$$\tilde{\mathbf{h}}^{(\theta+1)}(\mathbf{i}) = \mathcal{P}\left(\tilde{\mathbf{f}}^{(\theta)}(\mathbf{i})\right) \quad (68)$$

where θ refers to the iteration number, and $\mathcal{P}$ is the projection operator that projects the iterate into the constraint set $\mathcal{C}$, which is defined by (43). We use the convergence parameter $\alpha = 0.005$ in our simulations. The projection operator is defined as [20]

$$\mathcal{P}\left(\tilde{\mathbf{f}}^{(\theta)}(\mathbf{i})\right) \triangleq \tilde{\mathbf{f}}^{(\theta)}(\mathbf{i}) - \frac{1}{3|\mathcal{S}|}\left(\sum_{\mathbf{i}\in\mathcal{S}} \tilde{\mathbf{f}}^{(\theta)}(\mathbf{i}) - \tilde{\mathbf{I}}\right) \mathbf{1}\mathbf{1}^T. \quad (69)$$

C. Linear Color Model for the Human Visual System

To obtain a true matrix linear color model, one needs to model the color processing of the human visual system as a convolution with a matrix-valued filter $\tilde{\mathbf{v}}(\mathbf{m})$. The development of such a model is beyond the scope of this paper and a topic for future research. Instead, we use a pattern-color separable model for the human visual system based on the work of Poirson and Wandell [14], [21]. The pattern-color separable color vision model forms the basis for the S-CIELab color space, which has become an industry standard [22]. The pattern-color separable model first transforms device dependent RGB values (where R, G and B are coefficients of standard spectral tristimulus basis functions) into a space with basis functions represented by the normalized color sensitivities of the three fundamental cones responsible for human color vision. The three cones are called the L, M and S cones respectively, to denote long (L), medium (M), and short (S) wavelength sensitivities. Thus, at each pixel an RGB value is transformed into the corresponding cone photoreceptor absorption rates. The L, M, and S basis functions are referred to in the literature as the Smith–Pokorny cone fundamentals [23]. The LMS coordinates are then transformed using a color transformation into an opponent representation [24]. The three opponent visual pathways are the white−black (or the luminance pathway), red−green and blue−yellow pathways (chrominance pathways). The "−" in red−green and blue−yellow should be read as "minus" and not confused with a hyphen. Thus, white and black are in opposition, red and green are in opposition, and blue and yellow are in opposition. Such a representation is very different from early RGB models where it was believed that humans respond to the three primary colors [24]. Strong support for the opponent representation comes from the fact that humans do not perceive colors that are reddish green or yellowish blue since the red−green and yellow−blue visual pathways are opponent channels. Poirson and Wandell [14], [21] found that spatial frequency sensitivity to color patterns could be modeled as spatial frequency sensitivity of the three channels in the opponent representation.

Thus, the linear color model consists of

1) a linear transformation $\tilde{\mathbf{T}}$;
2) separable spatial filtering on each channel using a different spatial filter on each channel. This operation may be regarded as a matrix multiplication in the frequency domain by a diagonal matrix $\tilde{\mathbf{D}}(\mathbf{z})$.

Thus, $\mathbf{v}(\mathbf{m})$ is computed as

$$\mathbf{v}(\mathbf{m}) = \tilde{\mathbf{d}}(\mathbf{m})\tilde{\mathbf{T}}. \quad (70)$$

We now describe the computation of the model parameters for viewing RGB images on a monitor. First, one needs to account for the fact that the eight-bit values that are put in the frame buffer to trigger the red, green, and blue guns of the CRT are *not* the RGB tristimulus values of the colors displayed on the monitor. This is because the CRT has a nonlinear response to frame buffer values. Thus, we need to pass the RGB values of the image through this nonlinearity to obtain the RGB coordinates of the colors displayed on the monitor. This corresponds to the inverse of gamma correction. The color images are first preprocessed with this point-nonlinearity before they are halftoned. This ensures that the colors in the halftone are closest to the color actually rendered on the monitor.

The linear transformation $\tilde{\mathbf{T}}$ is computed as the composition of two linear transformations $\tilde{\mathbf{C}}$ and $\tilde{\mathbf{O}}$. The transformation $\tilde{\mathbf{C}}$ is the transformation that converts linear RGB values into Smith–Pokorny cone absorption rates. $\tilde{\mathbf{C}}$ is a monitor dependent transformation. The transformation $\tilde{\mathbf{O}}$ that transforms the LMS coordinates into the opponent representation is given in [14], [21], [22] and is monitor independent. The spatial frequency weighting functions for the three opponent visual pathways were obtained for viewing images displayed on the monitor at 72 dots per inch (dpi) at a "normal" viewing distance of 18 in using the parameters given in [22].

D. Simulation Results

Several random initial guesses were tried, and the descent algorithm was terminated when the changes in the objective function were below a predefined threshold. Using this method, one may explore different minimizers (solutions that result in nearly the same objective function value). The uniformity in the dot distributions produced by different initial guesses was different. It has been shown [25]–[27] that frequency weighted mean squared error alone cannot guarantee optimum dot distributions. This problem can be alleviated by using threshold modulation [28]. For the purpose of this work, since we are only concerned with the noise shaping behavior of error diffusion, we chose a solution that has a reasonably uniform dot distribution.

Our calibration data used a monitor display $\gamma \approx 2.2$, and a monitor dependent transformation matrix $\tilde{\mathbf{C}}$

$$\tilde{\mathbf{C}} = \begin{pmatrix} 2.0935 & 7.6018 & 1.1235 \\ 0.7921 & 7.6394 & 1.6264 \\ 0.0894 & 0.8020 & 7.6618 \end{pmatrix}. \quad (71)$$

The optimal filter coefficients obtained for this monitor were

$$\tilde{\mathbf{h}}(0,\,1) = \begin{pmatrix} 0.6316 & -0.1306 & 0.0323 \\ -0.0430 & 0.3993 & 0.0327 \\ -0.0167 & -0.1082 & 0.7379 \end{pmatrix}$$

$$\tilde{\mathbf{h}}(1,\,1) = \begin{pmatrix} -0.1949 & 0.1289 & -0.0242 \\ 0.0817 & -0.0730 & 0.0645 \\ 0.0454 & 0.1585 & -0.4017 \end{pmatrix}$$

$$\tilde{\mathbf{h}}(1,\,0) = \begin{pmatrix} 0.3598 & -0.0549 & 0.0403 \\ -0.0018 & 0.2906 & 0.0173 \\ -0.0080 & -0.0895 & 0.4867 \end{pmatrix}$$

$$\tilde{\mathbf{h}}(1,\,-1) = \begin{pmatrix} 0.2181 & -0.0112 & 0.0047 \\ 0.0222 & 0.1515 & 0.0580 \\ 0.0129 & 0.0213 & 0.1614 \end{pmatrix}.$$

The optimal filter that was obtained based on our calibrated color monitor and was tested on five standard color test images (*Lena, peppers, pasta, fruits, hats*). In each case, to evaluate the noise shaping behavior, we produced undistorted halftones using the color signal distortion canceling method developed in Section III-B2. Section III-B2 showed that according to the matrix gain model, the quantization error image in the distortion canceling method is in fact the uncorrelated noise injection into the halftoning system. Therefore, we used the error image produced while halftoning the set of test images with distortion canceling schemes using the Floyd–Steinberg error filter and the optimal filter, respectively, as the noise image in the objective function of (42). The effective noise shaping gain (in decibels) of the optimal filter over the separable Floyd–Steinberg filter may be computed as

$$NG = 10\log_{10}\left(\frac{J_{fs}}{J_{opt}}\right) \tag{72}$$

where the numerator and denominator in the argument of the log function are the objective functions computed by using (42) for the optimal filter and the Floyd–Steinberg filter, respectively. Sample averages were used to estimate the expectations. Table I tabulates the noise gain of the optimal filter over using a separable Floyd–Steinberg error filter.

Fig. 8(a) shows the *pasta* image halftoned using Floyd–Steinberg halftoning on each color plane. Fig. 8(b) shows a magnified view of a portion of the image. Fig. 9(a) and (b) show the corresponding results for halftoning with the optimal error filter. The optimal filter results in less visible halftone noise. It significantly reduces color impulses when compared with scalar error diffusion using filters with scalar coefficients. The halftone noise patterns produced by conventional Floyd–Steinberg error scalar filter were significantly more visible when observed on the calibrated monitor as compared to the noise patterns produced by the optimal filter.[1] However the proposed design procedure does not guarantee that the distribution of the color dots is the most regular possible. It must be emphasized that since the optimal filter coefficients are dependent on a particular monitor configuration, the above design process must be applied on a case-by-case basis. Since our color model is defined in a device independent color space, our preceding discussion holds for other color spaces as well. For example, if we are working in a Cyan–Magenta–Yellow (CMY) color space (for a printing application), then we can convert CMY into corresponding CIE XYZ coordinates [24] and then into the opponent representation. Thus, using a new color transformation matrix $\tilde{\mathbf{T}}$, the optimal filter for this case can be calculated using the method described in this section.

[1]Images available at http://signal.ece.utexas.edu/~damera/col-vec.html.

TABLE I
NOISE GAIN OF THE OPTIMAL FILTER ON STANDARD TEST IMAGES

image	Noise gain (dB)
lenna	3.2868
peppers	1.8775
fruits	1.3741
pasta	1.4563
hats	1.0452

V. PARALLEL IMPLEMENTATION OF THE ERROR FILTER

In this section, we show that an error filter with matrix-valued coefficients has a parallel implementation, which can increase throughput by up to a factor of three. A filter with matrix-valued coefficients can be implemented with *conventional* filtering operations applied in parallel to each component of the vector sequence being filtered.

Analyzing (5) and using $\mathbf{F}(\mathbf{z})$ for the z-transform of the feedback signal, we obtain

$$\begin{pmatrix} F_0(\mathbf{z}) \\ F_1(\mathbf{z}) \\ F_2(\mathbf{z}) \end{pmatrix} = \begin{pmatrix} H_{0,0}(\mathbf{z}) & H_{0,1}(\mathbf{z}) & H_{0,2}(\mathbf{z}) \\ H_{1,0}(\mathbf{z}) & H_{1,1}(\mathbf{z}) & H_{1,2}(\mathbf{z}) \\ H_{2,0}(\mathbf{z}) & H_{2,1}(\mathbf{z}) & H_{2,2}(\mathbf{z}) \end{pmatrix} \begin{pmatrix} E_0(\mathbf{z}) \\ E_1(\mathbf{z}) \\ E_2(\mathbf{z}) \end{pmatrix}. \tag{73}$$

We represent the filtering using Fig. 10. Each of the filters $H_{i,j}(\mathbf{z})$, $i, j = 0, 1, 2$, is a polyphase component of the multifilter, and represents a conventional scalar filter that can be derived from the filter coefficients of the multifilter $\tilde{\mathbf{h}}$ using the polyphase decomposition. In fact, $h_{i,j}(\mathbf{m}) = [\tilde{\mathbf{h}}(\mathbf{m})]_{i,j}$. Since $\tilde{\mathbf{h}}$ is fixed, the polyphase components of its rows may be precomputed. Nine polyphase filters are required for the implementation.

The result is a set of conventional filters with scalar coefficients, which enables the components of the input signal vector sequence to be buffered and filtered independently of the other components, in parallel. Since the filters $h_{i,0}$, $h_{i,1}$ and $h_{i,2}$ are operate in parallel, the parallel polyphase implementation is three times faster than a sequential implementation of (4). We may utilize three low-bandwidth, low-cost embedded processors instead of one high bandwidth processor to get the same performance at a lower cost [13] or use a processor with VLIW or SIMD parallel processing operations, such as the TMS320C6000 or Intel Pentium MMX, respectively. The parallel implementation does not require shared circular buffers. Each component of the input vector sequence is put into a separate circular buffer on each of the three parallel digital signal processors (DSPs). This allows for fast, low-overhead

(a)

(b)

Fig. 8. Performance of the separable Floyd–Steinberg filter. (a) *Pasta* halftoned with Floyd–Steinberg filter. (b) Magnified portion of halftone.

(a)

(b)

Fig. 9. Performance of the optimal filter. (a) *Pasta* halftoned with optimal filter. (b) Magnified portion of halftone.

loop code making the implementation efficient on parallel programmable DSPs.

VI. Conclusion

This paper formalizes the idea that error diffusion may be approximated as a system that produces frequency distortion and adds additive noise [29]. The modeling approach generalizes modeling methods for scalar error diffusion [3] to the vector case. We linearize vector error diffusion based on a "matrix gain model" for the quantizer that accounts for correlations among the components of the vector error being diffused. We use this modeling to predict the linear signal distortion and noise shaping effects of vector error diffusion. Based on the model, we derive a low-complexity compensation method to eliminate signal frequency distortion in vector error diffusion. The model could potentially be used for color halftone compression, in which one may decide to allocate bits according to the signal distortion and noise injection profiles predicted by the model.

We develop a model-based error filter design method in which the objective is to minimize the visual effect of the additive noise injection produced by vector error diffusion. We cast the optimal error filter design problem as a generalized weighted linear prediction problem and derived the set of equations that may be regarded as a generalization of the Yule–Walker equations. The solution of the generalized set of equations results in color error filters with visually optimum noise shaping. The explicit modeling for the human visual system incorporates a generalized linear spatially invariant matrix-valued weighting and is not restricted to the pattern-color separable model [14] that is used to obtain our filters. Thus, more general linear visual models could be used if they were available. Future work could explore the role of the constraints in designing optimal color error filters. Better results were obtained when the lossless diffusion constraints were not strictly observed. Symbolic optimization such as the approach of [30] could be used to explore constrained design spaces in an automated

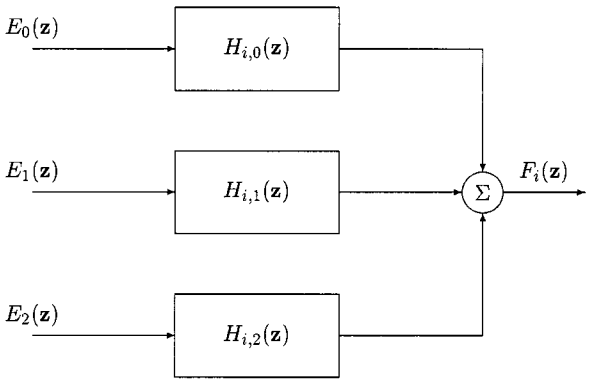

Fig. 10. Parallel polyphase structure for matrix valued error filter. Each output color component is obtained by filtering the color components of the inputs with different filters, each with scalar valued coefficients, and then combining their outputs. $i = 0, 1, 2$ correspond to the computation of the red, green, and blue components of the output, respectively.

framework where the error filter can be simultaneously optimized to satisfy several constraints.

Finally, we showed that the matrix-valued color error filters, when put into polyphase form, have an efficient parallel implementation. Such an implementation is especially valuable when using conventional embedded digital signal processor architectures.

REFERENCES

[1] R. Ulichney, *Digital Halftoning*. Cambridge, MA: MIT Press, 1987.

[2] K. Knox, "Error image in error diffusion," *Proc. SPIE*, vol. 1657, pp. 268–279, Feb. 1992.

[3] T. D. Kite, B. L. Evans, and A. C. Bovik, "Modeling and quality assessment of halftoning by error diffusion," *IEEE Trans. Image Processing*, vol. 9, pp. 909–922, May 2000.

[4] T. D. Kite, "Design and quality assessment of forward and inverse error-diffusion halftoning algorithms," Ph.D. dissertation, Dept. Elect. Comput. Eng., Univ. Texas, Austin, TX, Aug. 1998.

[5] J. Jarvis and C. Roberts, "A new technique for displaying continuous tone images on a bilevel display," *IEEE Trans. Commun.*, pp. 891–898, Aug. 1976.

[6] R. Floyd and L. Steinberg, "An adaptive algorithm for spatial grayscale," *Proc. Soc. Image Display*, vol. 17, no. 2, pp. 75–77, 1976.

[7] T. D. Kite, B. L. Evans, A. C. Bovik, and T. L. Sculley, "Digital halftoning as 2-D delta–sigma modulation," in *Proc. IEEE Conf. Image Processing*, vol. 1, Oct. 1997, pp. 799–802.

[8] S. Ardalan and J. Paulos, "An analysis of nonlinear behavior in delta–sigma modulators," *IEEE Trans. Circuits Syst.*, vol. CAS-34, pp. 593–603, June 1987.

[9] B. Kolpatzik and C. Bouman, "Optimized error diffusion for high quality image display," *J. Electron. Imag.*, vol. 1, pp. 277–292, Jan. 1992.

[10] L. Akarun, Y. Yardimici, and A. E. Cetin, "Adaptive methods for dithering color images," *IEEE Trans. Image Processing*, vol. 6, pp. 950–955, July 1997.

[11] B. Kolpatzik and C. Bouman, "Optimized error diffusion based on a human visual model," *Proc. SPIE*, vol. 1666, pp. 152–164, Feb. 1992.

[12] P. Wong and J. Allebach, "Optimum error diffusion kernel design," in *Proc. SPIE/IS&T Symp. Electronic Imaging*, Jan. 1997.

[13] G. Strang and T. Q. Nguyen, *Wavelets and Filter Banks*. Cambridge, MA: Wellesley-Cambridge Press, 1996.

[14] A. B. Poirson and B. A. Wandell, "Appearance of colored patterns: Pattern-color separability," *J. Opt. Soc. Amer. A*, vol. 10, pp. 2458–2470, Dec. 1993.

[15] H. Stark and J. W. Woods, *Probability, Random Processes and Estimation Theory for Engineers*. Englewood Cliffs, NJ: Prentice-Hall, 1986.

[16] T. D. Kite, "Personal communication," unpublished, Sept. 25, 1999.

[17] T. K. Moon and W. C. Stirling, *Mathematical Methods and Algorithms for Signal Processing*. Englewood Cliffs, NJ: Prentice-Hall, 2000.

[18] N. Damera-Venkata, "Analysis and design and of vector error diffusion systems for image halftoning," Ph.D. dissertation, Dept. Elect. Comput. Eng., Univ. Texas, Austin, TX, Dec. 2000.

[19] P. L. Combettes and P. Bondon, "Adaptive linear filtering with convex constraints," in *Proc. IEEE Int. Conf. Acoustics, Speech, Signal Processing*, vol. 2, May 1995, pp. 1372–1375.

[20] H. Stark and Y. Yang, *Vector Space Projections*. New York: Wiley, 1998.

[21] A. B. Poirson and B. A. Wandell, "Pattern-color separable pathways predict sensitivity to simple colored patterns," *Vis. Res.*, vol. 36, pp. 515–526, Dec. 1996.

[22] X. Zhang and B. A. Wandell, "A spatial extension of CIELab for digital color image reproduction," in *SID Tech. Dig.*, 1996, pp. 731–734.

[23] V. Smith and J. Pokorny, "Spectral sensitivity of the foveal cone photopigments between 400 and 500 nm," *Vis. Res.*, vol. 15, pp. 161–171, 1975.

[24] M. D. Fairchild, *Color Appearance Models*. Reading, MA: Addison-Wesley, 1998.

[25] P. Wong, "Image halftoning using multipath tree coding," in *Proc. IEEE Conf. Image Processing*, vol. 2, Nov. 1994, pp. 31–35.

[26] ——, "Entropy constrained halftoning using multipath tree coding," *IEEE Trans. Image Processing*, vol. 6, pp. 1567–1569, Nov. 1997.

[27] ——, "Adaptive error diffusion and its application in multiresolution rendering," *IEEE Trans. Image Processing*, vol. 5, pp. 1184–1196, July 1996.

[28] K. Knox and R. Eschbach, "Threshold modulation in error diffusion," *J. Electron. Imag.*, vol. 2, pp. 185–192, July 1993.

[29] N. Damera-Venkata, T. D. Kite, W. S. Geisler, B. L. Evans, and A. C. Bovik, "Image quality assessment based on a degradation model," *IEEE Trans. Image Processing*, vol. 9, pp. 636–651, Apr. 2000.

[30] N. Damera-Venkata and B. L. Evans, "An automated framework for multicriteria optimization of analog filter designs," *IEEE Trans. Circuits Syst. II*, vol. 46, pp. 981–990, Aug. 1999.

Niranjan Damera-Venkata (M'00) was born in Madras, India, in December 1976. He received the B.E. degree in electronics and communication engineering (ranking third in the University) from the University of Madras, in July 1997 and the M.S. and Ph.D. degrees in electrical engineering from The University of Texas at Austin in May 1999 and December 2001, respectively.

Since July 2000, he has been with the Imaging Technology Department, Hewlett-Packard Research Laboratories, Palo Alto, CA, where he is currently a Research Engineer. His research interests are in the general area of signal and image processing and currently include, document image processing, symbolic design and analysis tools, image and video quality assessment, and digital camera image processing.

Dr. Damera-Venkata is a member of Sigma Xi. He won a 1998–1999 Texas Telecommunications Engineering Consortium Graduate Fellowship from The University of Texas.

Brian L. Evans (S'88–M'93–SM'97) received the B.S.E.E.C.S. degree from the Rose-Hulman Institute of Technology, Terre Haute, IN, in May 1987, and the M.S.E.E. and Ph.D. degrees from the Georgia Institute of Technology, Atlanta, in December 1988 and September 1993, respectively.

From 1993 to 1996, he was a Postdoctoral Researcher at the University of California, Berkeley, where he worked on electronic design automation for embedded systems as a member of the Ptolemy project. He is the primary architect of the Signals and Systems Pack for Mathematica, which has been on the market since October of 1995. He is currently a tenured Associate Professor with the Department of Electrical and Computer Engineering with The University of Texas at Austin. He enjoys conducting research and teaching courses in embedded real-time signal and image processing systems. His current research focuses on the design and real-time implementation of ADSL/VDSL transceivers, desktop printer pipelines, video codecs, and 3-D sonar imaging systems. He developed and currently teaches multidimensional digital signal processing, embedded software systems, and real-time digital signal processing laboratory.

Dr. Evans is an Associate Editor of the IEEE TRANSACTIONS ON IMAGE PROCESSING, a member of the Design and Implementation of Signal Processing Systems Technical Committee of the IEEE Signal Processing Society, and the recipient of a 1997 National Science Foundation CAREER Award.